Section 3 Auditory Physiology

Chapter 1 Signal Transmission in the Auditory System

Chapter 1. Signal Transmission in the Auditory System

Academic and Research Staff

Professor Dennis M. Freeman, Professor Lawrence S. Frishkopf, Professor Nelson Y-S. Kiang, Professor William T. Peake, Professor Thomas F. Weiss, Dr. Colette S. Boex-Spano, Dr. Peter A. Cariani, Dr. Bertrand Delgutte, Dr. Donald K. Eddington, Dr. John J. Guinan, Jr., Dr. M. Charles Liberman, Dr. William M. Rabinowitz, Dr. Christopher A. Shera, Marc A. Zissman

Visiting Scientists and Research Affiliates

Dr. Robert D. Hall, Dr. Ruth Y. Litovsky, Dr. Sunil Puria, Michael E. Ravicz, Dr. John J. Rosowski, Joseph Tierney

Graduate Students

C. Cameron Abnet, Alexander J. Aranyosi, C. Quentin Davis, Benjamin M. Hammond, Shilpa M. Hattangadi, Gregory T. Huang, John R. Iversen, Laura K. Johnson, Sridhar Kalluri, Zoher Z. Karu, Leonid M. Litvak, Christopher J. Long, Srijoy Mahapatra, Martin F. McKinney, Pankaj Oberoi, Mark N. Oster, Anthony D. Patire, Rosanne Rouf, Lisa F. Shatz, Konstantina M. Stankovic, Thomas M. Talavage, Su W. Teoh, Emily M. Tsai, Susan E. Voss

Technical and Support Staff

Janice L. Balzer, David A. Steffens

1.1 Introduction

Research on the auditory system is carried out in cooperation with two laboratories at the Massachusetts Eye and Ear Infirmary (MEEI). Investigations of signal transmission in the auditory system involve the Eaton-Peabody Laboratory for Auditory Physiology, whose long-term objectives are (1) to determine the anatomical structures and physiological mechanisms that underlie vertebrate hearing, and (2) to apply this knowledge to clinical problems. Studies of cochlear implants in humans are carried out at MEEI's Cochlear Implant Research Laboratory. Cochlear implants electrically stimulate intracochlear electrodes to elicit patterns of auditory nerve fiber activity that the brain can learn to interpret. The ultimate goal for these devices is to provide speech communication for the profoundly deaf.

1.2 Middle and External Ear

Sponsors

National Institutes of Health
Grant R01-DC-00194
Grant P01-DC-00119

Project Staff

Dr. John J. Rosowski, Professor William T. Peake, Dr. Sunil Puria, Greg T. Huang, Michael E. Ravicz, Su W. Teoh, Susan E. Voss

1.2.1 Overall Goal

Our aim is to determine how the structure of normal and pathological external and middle ears affect their acoustic and mechanical functions. We measure the workings of ears of various animals as well as normal and pathologic human middle ears. Acoustic and mechanical measurements along with structural measurements are used to generate testable quantitative models of external and middle-ear function. This knowledge is applied to practical issues such as providing specifications for reconstructive surgery of human ears. Knowledge integrated across animal species can lead to connections of the ear's structure and function with ecological variables such as habitat. Thus, hypotheses about the processes involved in the evolution of the ear can be tested.

1.2.2 Middle-Ear Structure and Function

Last year, our studies of the structure and function of the middle-ears of different animals followed four paths: (1) tests of the common assumption that the cochlea responds to the difference in sound pressure at the two cochlear windows, (2) measurements of the acoustic function of an anatomically distinct section of the tympanic membrane, the *pars flaccida*, (3) an analysis of acoustic power flow through the external and middle ear in gerbils, and (4) a study of how the size of the ear effects middle-ear function.

The first study confirmed that the window pressure difference is the primary cochlear input; this study was the subject of a Master's thesis and a submitted paper. The second study resulted in the first demonstration of a role for *pars flaccida* in limiting the low-frequency response of the middle ear and was the subject of another Master's thesis. The third study, the subject of a paper in press, demonstrated that the power-collection performance of the gerbil external and middle ear plays a large role in determining the overall shape of the gerbil audiogram. The fourth study compared middle-ear function in ears of similar structure, but greatly different size: the ears of house cats and a lion. This work led to a quantitative rule relating skull length and middle-ear cavity function that was the subject of a meeting presentation.

In earlier work, we have used acoustic theory to determine how the sound-power delivered to the middle ear is related to the incident power density in a diffuse acoustic field. The ratio of these power measures, the "effective area" of the ear, can be expressed in terms of two acoustic impedances (one impedance looking into the middle ear, and one looking out from the middle ear through the external ear) and an acoustic power efficiency (associated with the external ear). Determination of this effective area as a function of frequency is then a complete description of the ear's performance in capturing acoustic power in a diffuse field.[1]

This approach has been applied to gerbil ears through the use of measurement of the two relevant impedances and a theoretical determination of the external-ear efficiency, based on a model that mimics both the external ear geometry and its radiation impedance measurement.[2] This framework has been used to test the hypothesis that the behavioral threshold for detection of a tone by a gerbil corresponds to a fixed level of power input to the ear. The analysis shows that threshold corresponds to power absorption of 5×10^{-17} watts over more than two decades of frequency (0.1-20 kHz).

The acoustic input impedance of the inner ear is the acoustic "load" that is driven by the middle ear; knowledge of this impedance is an essential component to understanding sound transmission to the inner ear. Though measurements have been made of this quality in cat ears, until recently no direct measurement existed for human ear. Building on previous experience with measurements in human cadaver ears, new measurements in 12 human ears have established the nature of this impedance, which will provide guidance for construction of prosthesis and a constraint on theories of inner ear mechanisms.[3]

Our earlier work on analysis of mechanisms involved in hearing for ears with major disfunction of the ossicular chain has led both to new experiments that test the accuracy of a crucial assumption and to experiments that apply the ideas to surgical procedures and clinical assesment of efficacy. From measurements in cat ears, we have shown that the assumption that the inner ear responds to sound-pressure *difference* between its two connections with the middle ear is quite accurate with a "common-mode rejection" ratio of about 40 dB over the frequency range tested.[4] In cooperation with Dr. Saumil Merchant, a surgeon on the Massachusetts Eye and Ear staff, experimental tests on human cadaver ears and clinical trials of modifications in reconstructive procedures are proceeding.

---

1 J.J. Rosowski, "Models of External and Middle-ear Function," in *The Springer Handbook on Auditory Research*, eds. H.L. Hawkinds, T.A. McMullen, A.N. Popper, and R.R. Fay (New York: Springer-Verlag, 1996).

2 M.E. Ravicz, J.J. Rosowski, and H.F. Voigt, "Sound-power Collection by the Auditory Periphery of the Mongolian Gerbil *Meriones* Unguiculatus II External-ear Radiation Impedance and Power Collection," *J. Acoust. Soc. Am.* 99: 3044-3063 (1996).

3 S.N. Merchant, M.E. Ravicz, and J.J. Rosowski, "Acoustic Input Impedance of the Stapes and Cochlea in Human Temporal Bones," *Hear. Res.* 97: 30-45 (1996).

4 S.E. Voss, J.J. Rosowski, and W.T. Peake, "Is the Pressure Difference between the Oval and Round Windows the Effective Acoustic Stimulus for the Cochlea?" *J. Acoust. Soc. Am.* 100: 1602-1616 (1996).

1.2.3 Publications

Published Journal Articles

Huang, G.T., J.J. Rosowski, D.T. Flandermeyer, and W.T. Peake. "Middle Ear of a Lion: A Comparison of Structure and Function to Domestic Cat." *J. Acoust. Soc. Am.* 99: 2562 (1996).

Merchant, S.N., M.E. Ravicz, and J.J. Rosowski. "Acoustic Input Impedance of the Stapes and Cochlea in Human Temporal Bones." *Hear. Res.* 97: 30-45 (1996).

Ravicz, M.E., J.J. Rosowski, and H.F. Voigt. "Sound-power Collection by the Auditory Periphery of the Mongolian Gerbil *Meriones* Unguiculatus: II. External-ear Radiation Impedance and Power Collection." *J. Acoust. Soc. Am.* 99: 3044-3063 (1996).

Voss, S.E., J.J. Rosowski, and W.T. Peake. "Is the Pressure Difference between the Oval and Round Windows the Effective Acoustic Stimulus for the Cochlea?" *J. Acoust. Soc. Am.* 100: 1602-1616 (1996).

Journal Articles, Submitted

Cherukupally, S.R., S.N. Merchant, and J.J. Rosowski. "Correlates between Stapes Pathology and Conductive Hearing Loss in Otosclerosis." Submitted to *Ann. Otol. Rhinol. Laryngol.*

Gopen, Q., J.J. Rosowski, and S.N. Merchant. "Anatomy of the Normal Human Cochlear Aqueduct with Functional Implications." Submitted to *Hear. Res.*

Puria, S., J.J. Rosowski, and W.T. Peake. "Measurements of Middle-ear Pressure Gain in Human Temporal Bones." Submitted to *J. Acoust. Soc. Am.*

Whittemore, K.R., S.N. Merchant, and J.J. Rosowski. "Acoustic Mechanisms: Canal Wall-up versus Canal Wall-down Mastiodectomy." Submitted to *Archives Otolaryngol. - Head and Neck Surgery.*

Chapter in a Book

Rosowski, J.J. "Models of External and Middle-ear Function." In *The Springer Handbook on Auditory Research.* pp. 15-61. Eds. H.L. Hawkins, T.A. McMullen, A.N. Popper, and R.R. Fay. New York: Springer-Verlag, 1996, Volume 6: *Auditory Computation.*

Conference Papers

Merchant, S.N., M.E. Ravicz, and J.J. Rosowski. "Temporal Bone Model of Type IV Tympanoplasty." *Abstracts of the 19th Midwinter Meeting of the Association for Research in Otolaryngology*, p. 54.

Ravicz, M.E., S.E. Voss, S.N. Merchant, and J.J. Rosowski. "An Upper Bound on the Compressibility of the Human Cochlea." *Abstracts of the 19th Midwinter Meeting of the Association for Research in Otolarngology*, 1996, p. 57.

Rosowski, J.J., and A. Dobrzeniecki. "Computer-assisted Three-dimensional Reconstructions of Normal and Pathological Human Middle Ears." *Abstracts of the 19th Midwinter Meeting of the Association for Research in Otolarngology*, 1996, p. 204.

Teoh, S-W., D.T. Flandermeyer, and J.J. Rosowski. "The Effect of *Pars Flaccida* of the Tympanic Membrane on Hearing Function." *Abstracts of the 19th Midwinter Meeting of the Association for Research in Otolarngology*, 1996, p. 196.

Whittemore, K.R., S.N. Merchant, and J.J. Rosowski. "The Effect of Manipulation of the *Aditus ad antrum* and Mastoid Air Cells on the Middle-ear Input Admittance." *Abstracts of the 19th Midwinter Meeting of the Association for Research in Otolaryngology*, 1996, p. 196.

1.3 Cochlear Mechanisms

Sponsors

Charles S. Draper Laboratory
Contract DL-H-496015
National Institutes of Health
Grant R01 DC00238

Project Staff

Professor Thomas F. Weiss, Professor Dennis M. Freeman, C. Cameron Abnet, Alexander J. Aranyosi, C. Quentin Davis, Laura K. Johnson, Zoher Z. Karu, Srijoy Mahapatra, Anthony D. Patire, Rosanne Rouf, Lisa F. Shatz

1.3.1 Osmotic Properties of the Tectorial Membrane

Osmotic responses obtained by observing changes in its shape and volume have revealed that the tectorial membrane (TM) behaves as a polyelectrolyte gel. Preliminary results of several of these studies have been described in previous *RLE Progress Reports*. During this year, we completed a study of the effects of changes in pH on the TM,[5] as well as a theoretical study that applied the theory of gels to the TM.[6]

1.3.2 Sound-induced Motions of Cochlear Structures

We have measured the motions of inner ear structures with a computer microvision system that has been described in previous progress reports. The system combines video microscopy, stroboscopic illumination, and computer vision algorithms.

We illustrate the capability of the system to measure three-dimensional sound-induced motion of an auditory receptor organ. We used an *in vitro* preparation of the alligator lizard cochlea and stimulated it hydrodynamically. To characterize three-dimensional motions, a time sequence of eight 3D-images were analyzed. The cochlea was stimulated with a 513 Hz, 92 dB SPL tone. Three-dimensional motions were estimated in a regular array of regions of the cochlea (figure 1).[7] Estimates of motion in all three directions were binned in the longitudinal (y) direction and plotted as a function of the distance from the neural edge of the cochlea (x direction). These results show that motions in the direction known to excite hair cells (x) were largest, between 400 and 500 nm peak-to-peak. Longitudinal motions, which have been shown to excite hair cells minimally, were an order of magnitude smaller. Transverse motions (z) increased abneurally, which is consistent with a functional interpretation of anatomy as well as with previous observation.[8]

The most compliant area of the basilar membrane (BM) is just abneural to the papilla; thus the abneural side will have the largest transverse motions. The magnitude of the transverse motion at this frequency is also consistent with previous measurements *in vivo*.[7]

1.3.3 Mechanical Properties of the Tectorial Membrane

The tectorial membrane (TM) is an important structure in the cochlea whose mechanical properties are not known. Understanding these properties will help us understand the mechanical forces that stimulate hair cells.

As reported in our progress report of last year, we have developed a method to investigate the mechanical properties of the TM. In this method, a portion of the TM, typically 350 μm in length, 100 μm in width, and 40 μm thick, is removed from the cochlea of a mouse. One surface of the TM is attached to the bottom of a glass chamber with tissue adhesive, and a single magnetizable bead (20 μm diameter, 6 percent SiFe) is attached to the free surface (figure 2).

---

5 D.M. Freeman, S.M. Hattangadi, and T.F. Weiss, "Osmotic Responses of the Isolated Mouse Tectorial Membrane to Changes in pH." *Aud. Neurosci.*, forthcoming.

6 T.F. Weiss and D.M. Freeman. "Equilibrium Behavior of an Isotropic Polyelectrolyte Gel Model of the Tectorial Membrane: the Role of Fixed Charges." *Aud. Neurosci.* Forthcoming.

7 W.T. Peake and A.L. Ling. "Basilar-membrane Motion in the Alligator Lizard: Its Relation to Tonotopic Organization and Frequency Selectivity." *J. Acoust. Soc. Am.* 67: 1736-1745 (1980).

8 T. Holton and A.J. Hudspeth, "A Micromechanical Contribution to Cochlear Tuning and Tonotopic Organization," *Sci.*, 222: 508-510 (1983); L.S. Frishkopf and D.J. DeRosier, "Mechanical Tuning of Free-standing Stereociliary Bundles and Frequency Analysis in the Alligator Lizard Cochlear," *Hear. Res.* 12: 393-404 (1983).

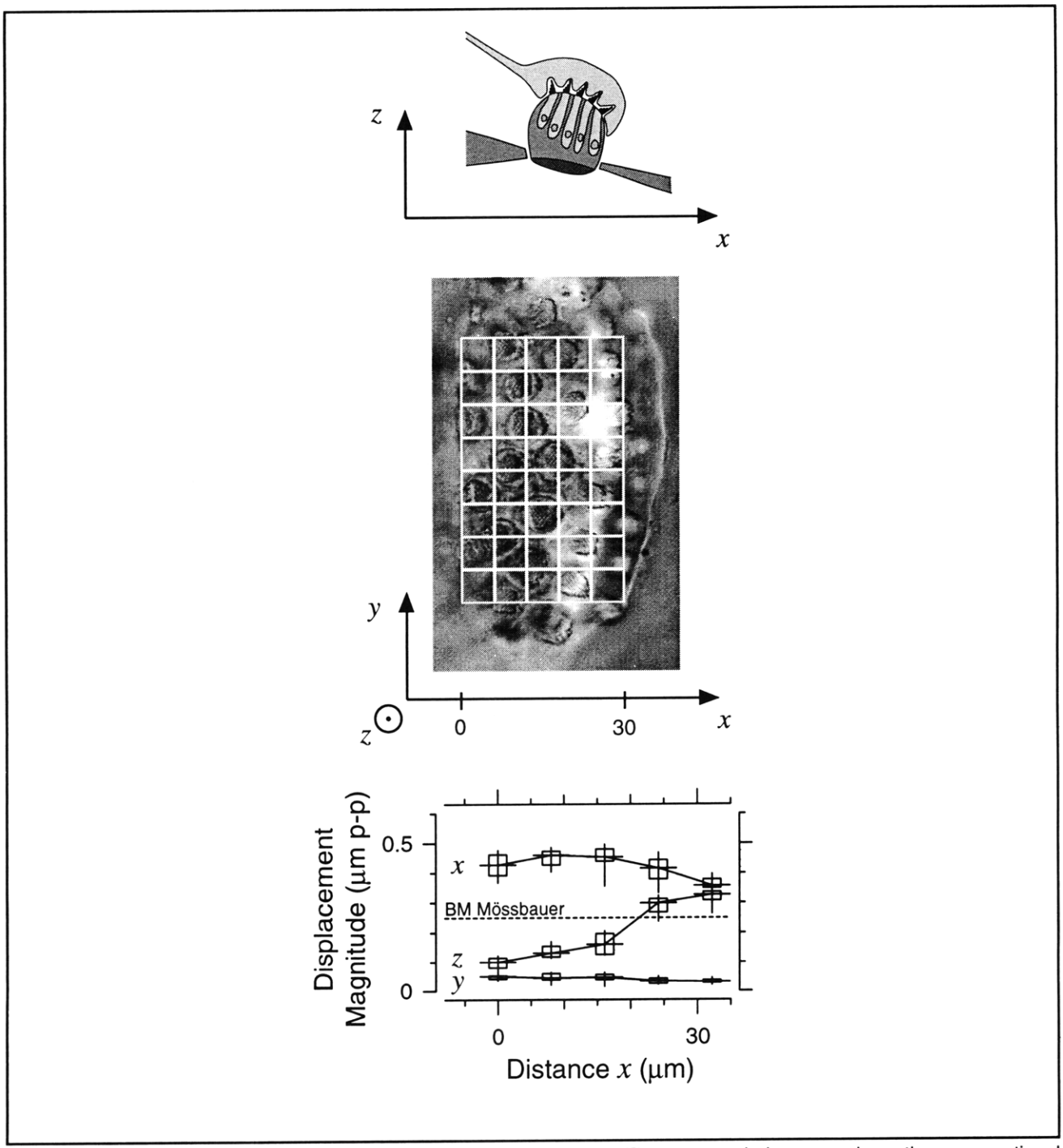

Figure 1. Three-dimensional motions of the alligator lizard cochlea. The top panel shows a schematic cross-sectional view of the inner ear of the lizard; a patch of five hair cells are shown resting on the basilar membrane with their hair bundles protruding into the overlying tectorial membrane. Video images were acquired at 13 planes of section separated by 3 μm and at eight phases of the sinusoidal stimulus (513 Hz tone, 92 dB SPL in the fluid adjacent to the basilar membrane). The center panel illustrates a typical image. Three-dimensional motions were estimated in 40 regions of interest, located on a regular grid (white lines). The magnitudes of the motion in the x, y, and z directions are plotted as a function of distance x from the neural edge of the papilla. The horizontal dashed line shows the measured motion of the basilar membrane in the transverse (z) direction obtained with the Mössbauer technique.

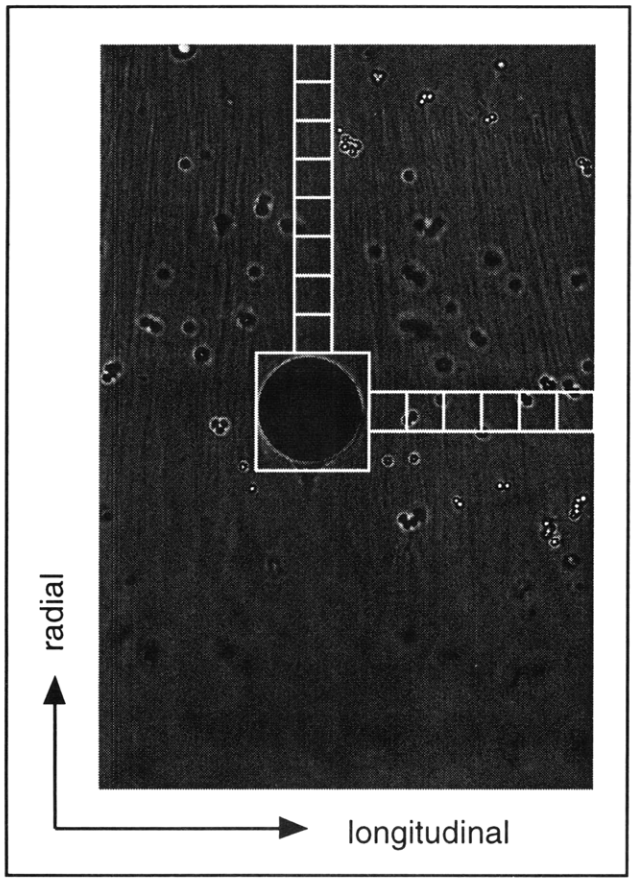

Figure 2. Image of the isolated TM preparation. The TM contains radially oriented fibrils seen as alternating light and dark striations in the image. The dark circle in the center of the image is a magnetizable bead (20 μm diameter, 6 percent SiFe) attached to the surface of the TM. The smaller dots are non-magnetic marker beads (1 μm diameter, polystyrene). Motions were estimated in the large white square which defines a region enclosing the magnetizable bead and in the smaller white squares which define adjacent regions.

The membrane and bead are placed in a magnetic field generated by computer-controlled electromagnets. The magnetic field induces a force on the bead which is transmitted to the membrane. By rotating the TM relative to the magnets, the direction of the force can be varied. The resulting motion of the bead and deformation of tissue regions near the bead are measured using a video microscopy system.

In preliminary measurements from seven tectorial membrane samples, we have compared the displacments that result from forces in the radial and longitudinal directions. The plots in figure 3 show the measured bead displacement for sinusoidal forces with amplitudes ranging from 0.02 to 1 μN. The displacements resulting from the longitudinally applied forces were consistently larger than those for radially applied forces. Furthermore, the relation between force and displacement is more nearly linear for longitudinal forces (slope = 0.90) than for radial forces (slope = 0.68). These results suggest that mechanical properties of the TM are not isotropic and that the anisotropy correlates with the structural anisotropy. The TM is both stiffer, and the point impedance is more markedly nonlinear when measured in a direction parallel to the radial fibrillar structure than in the orthogonal direction.

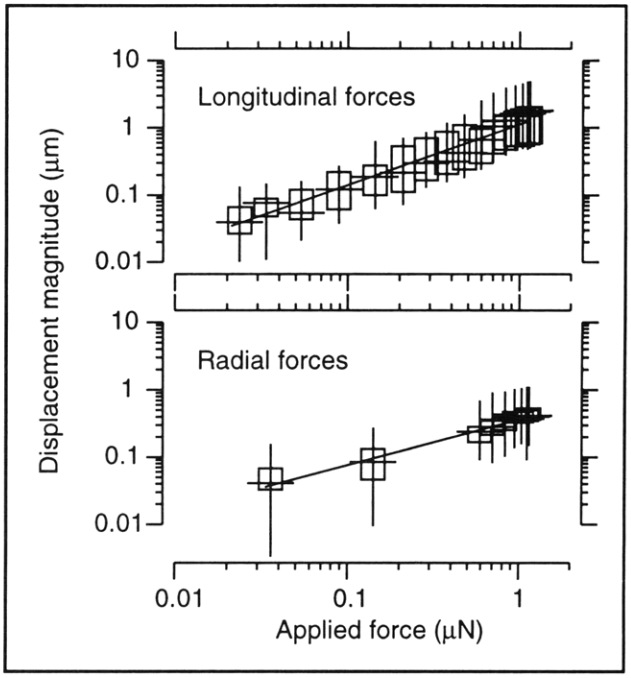

Figure 3. Displacement of a magnetizable bead as a function of applied force. Sinusoidal forces (10 Hz) with amplitudes between 0.02 and 1 μN were applied to a magnetizable bead that was attached to the surface of an isolated TM. Displacements of the magnetizable bead were determined from a sequence of video images obtained at different phases of the motion using stroboscopic illumination. Results are shown for forces directed in the longitudinal (top panel) and radial (bottom panel) directions for 7 tectorial membranes. Results at each amplitude are summarized by the median (horizontal line), range (vertical line), and the interquartile range (box). The slopes of regression lines through these data are 0.90 and 0.68 for longitudinal and radial forces, respectively.

The spatial extent of the deformation caused by the force applied to the bead can be estimated by measuring the motion of the TM as a function of the distance from the magnetizable bead (figure 4).

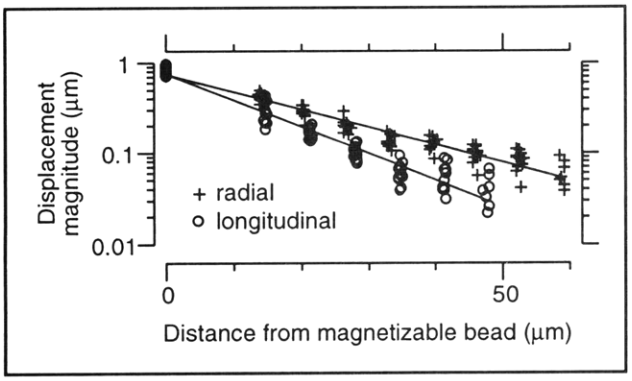

Figure 4. Motion of the magnetizable bead and the adjacent TM at a series of equally spaced points extending in the longitudinal and radial directions from the magnetizable bead. The force on the magnetizable bead was 0.8 μN at 10 Hz, and motions were measured at the locations indicated by white squares in figure 2. The solid lines are least-squares fits to the semi-log plots. The space constants in the longitudinal and radial directions are 14 and 22 μm respectively.

The displacement decreases more rapidly in the longitudinal than in the radial direction. This implies less mechanical coupling in the longitudinal direction. This anisotropy is once again consistent with the structural anisotropy of the TM.

1.3.4 Measuring Motions of a Microfabricated Gyroscope

In collaboration with Draper Laboratory, we have used the computer microvision system to measure three-dimensional motions of the microfabricated tuning-fork gyroscope developed at Draper. Two masses are supported by a system of cantilever springs. Integrated electrostatic drives induce a tuning-fork mode of motion in which each mass moves alternately toward and then away from the other. Rotations of the substrate about the line of symmetry between the masses give rise to Coriolis forces that tend to move the masses in oppositely-directed out-of-plane directions. Our goal is to measure the three-dimensional motions of the gyroscope and to characterize modes of motion that limit the sensitivity of the gyroscope (e.g., out-of-plane modes of motion that are not related to substrate rotation).

Figure 5 illustrates motion measurements that were obtained using our computer microvision system. Motions were excited by applying a sinusoidal voltage to the electrostatic drives of the gyroscope. Stroboscopic illumination, phase-locked to the sinusoidal voltage, was used to obtain images at eight evenly-spaced phases of the sinusoidal stimulus. The images were analyzed to determine the magnitude and phase of motion. The measurements, which were obtained at frequencies from 500 Hz to 22 kHz, demonstrate that the computer microvision system is capable of measuring motions over the entire range of frequencies important for the dynamics of the gyroscope. Each measurement was repeated five times to assess measurement noise. The standard deviation of the magnitude of the displacements is on the order of 5 nm at most frequencies. The standard deviation of the phase is typically less than 5 degrees.

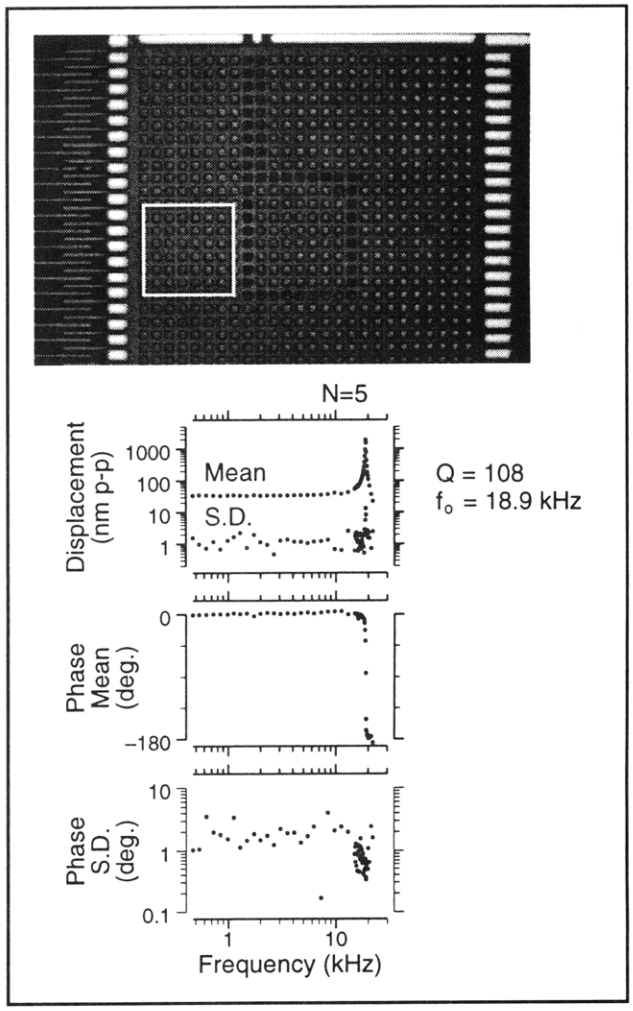

Figure 5. Frequency response. The top panel shows an image of Draper's microfabricated gyroscope that was taken using our computer microvision system. Motions of the gyroscope were excited by applying a sinusoidal voltage to the electrostatic comb drives (20 V AC plus a 20 V DC bias). The plots show the magnitude and phase of the resulting in-plane motion within the analysis region (white box in top panel) as a function of input frequency. Both the mean and standard deviation (S.D.) are plotted for five independent measurements.

To measure three-dimensional motions, sequences of images were obtained not only at the plane of sharpest focus but also at adjacent planes of focus

(figure 6). Results show that all three components of the motion of a moving tooth of the electrostatic comb drive were significantly above the noise floor of the measurement. The intended motions, which are parallel to the teeth, were more than 100 times larger than orthogonal motions in the plane of the substrate. Furthermore, the orthogonal motions could be smaller than these measurements suggest, since misalignment of the CCD camera and gyroscope (by less than one degree) could account for these measurements even if there were no orthogonal motion. Out-of-plane motions were less than a factor of 25 smaller than motions in the intended direction.

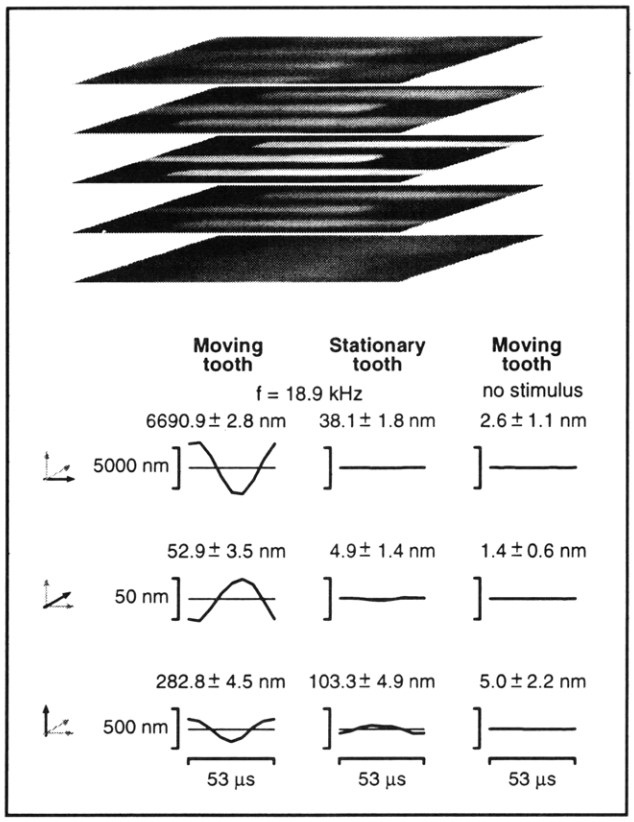

Figure 6. Out-of-plane motions. The gyroscope was driven at resonance (18.9 kHz) and images were obtained at eight evenly spaces phases of the sinusoidal stimulus and at 30 planes of focus separated by 1 μm. The top panel shows portions of five of the images (separated by 7 μm) enclosing three teeth in one of the comb drives. The plots show time waveforms for all three components of the motions of one tooth. The first and second columns show results for a tooth connected to the mass (moving) and for a tooth connected to the substrate (stationary). The third column shows results from a control experiment in which images of the moving tooth were analyzed when the stimulus was disconnected. Each test was repeated five times, and results are indicated as the mean ± standard deviation.

The accuracy of these measurements was assessed in three ways. First, each test was repeated five times to determine repeatability. The standard deviations were always less than 5 nm. Second, motions were also estimated for a tooth that was attached to the substrate. In-plane motions of this "stationary" tooth were much less than 1 percent of the corresponding motions of a moving tooth. However, out-of-plane motions were less than a factor of three smaller. These results suggest that motions of the nearby moving tooth are interfering with measurements of the stationary tooth. Lastly, motions were measured with the stimulus disconnected, and all the measurements were smaller than 5 nm. These results suggest that motions of nearby structures confound motion measurements using computer microvision. We are currently investigating computer vision algorithms to reduce the effect of motions of nearby structures.

1.3.5 Published papers

Journal Articles

Freeman, D.M., S.M. Hattangadi, and T.F. Weiss. "Osmotic Responses of the Isolated Mouse Tectorial Membrane to Changes in pH." *Aud. Neurosci.* Forthcoming.

Weiss, T.F., and D.M. Freeman. "Equilibrium Behavior of an Isotropic Polyelectrolyte Gel Model of the Tectorial Membrane: the Role of Fixed Charges." *Aud. Neurosci.* Forthcoming.

Conference Papers

Abnet, C.C., and D.M. Freeman. "Mechanical Properties of the Isolated Mouse Tectorial Membrane." *Abstracts of the 20th Midwinter Research Meeting of the Association for Research in Otolaryngology*, St. Petersburg Beach, Florida, February 2-6, 1997.

Davis, C.Q., and D.M. Freeman, "Using Video Microscopy to Measure 3D Cochlear Motions with Nanometer Precision." *Abstracts of the 20th Midwinter Research Meeting of the Association for Research in Otolaryngology*, St. Petersburg Beach, Florida, February 2-6, 1997.

Freeman, D.M., and C.Q. Davis. "Using Video Microscopy to Characterize Micromechanics of Biological and Manmade Micromachines." Invited paper at the Solid-State Sensor and Actuator Workshop, Hilton Head, South Carolina, June 3-6, 1996.

Freeman, D.M., S.M. Hattangadi, and T.F. Weiss. "Osmotic Responses of the Isolated Mouse Tectorial Membrane," *Abstracts of the 19th Midwinter Research Meeting of the Association for Research in Otolaryngology*, St. Petersburg Beach, Florida, February 4-8, 1996.

Weiss, T.F., and D.M. Freeman. "Isotropic Polyelectrolyte Gel Model of the Tectorial Membrane." *Abstracts of the 19th Midwinter Research Meeting of the Association for Research in Otolaryngology*, St. Petersburg Beach, Florida, February 4-8, 1996.

1.4 Auditory Neural Processing of Speech

Sponsor

National Institutes of Health
Grant R01-DC02258
Grant T32-DC00038

Project Staff

Dr. Bertrand Delgutte, Dr. Peter A. Cariani, Sridhar Kalluri, Benjamin M. Hammond, Emily M. Tsai

The long-term goal of our research is to determine how speech is coded in brainstem auditory nuclei, particularly the inferior colliculus (IC). Our work during the past year has focused on three questions: (1) How the limited dynamic range of auditory-nerve fibers affects their ability to accurately encode spectral patterns in their average rates of discharge, (2) how amplitude modulations in speech are encoded in neural discharge patterns, and (3) developing functional models of the response of brainstem auditory neurons to speech.

1.4.1 Neural Endoding of Spectral Patterns and the Dynamic Range Problem

The "dynamic range problem," the disparity between the wide range of intensities over which subjects show good speech and intensity discrimination and the narrow range over which single auditory-nerve fibers can encode intensity by their mean discharge rate, poses a challenge for theories of intensity discrimination and vowel perception. Modeling studies have concluded that rate codes can account for psychophysical performance even when spread of neural excitation to characteristic frequencies (CF) far from the signal frequency is limited by band-reject noise. However, these studies ignore the possible effects of the noise on the responses of neurons with CFs within the rejection band.

We have measured rate-level functions of auditory-nerve fibers in anesthetized cats for tone-burst stimuli presented both alone and in band-reject noise whose rejection band included the fiber CF. For moderate noise levels, the noise shifted rate-level functions horizontally towards high intensities, an effect likely due to suppression. For each increment in noise level by 1 dB, the rate-level function shifted by 0.5-1 dB (median 0.76 dB). Hence, the fiber could largely compensate for the noise in encoding tone intensity. However, for high noise levels, the benefit of this compensation was offset by large increases in minimum rate and decreases in maximum rate.

Our finding of a considerable effect of band-reject noise on the responses of auditory-nerve fibers has important implications for theories of intensity discrimination and vowel perception. In particular, the significant shifts in rate-level functions suggest that rate codes may perform even better than previously thought when spread of neural excitation is restricted by band-reject noise.

1.4.2 Neural Encoding of Amplitude Modulations in Speech

The temporal envelope of speech contains low-frequency (< 20 Hz) modulations that are essential for accurate reception. Our research is aimed at characterizing the representation of the amplitude envelope of speech in auditory neurons. This specification would allow for the design of speech processors (e.g., for cochlear implants) that accurately simulate the speech response envelope observed in the normal auditory system. In addition, this research may lead to a better understanding of how noise and reverberation degrade speech intelligibility.

We have recorded the activity of single units in the auditory nerve (AN), cochlear nucleus (CN), and inferior colliculus (IC) of dial-anesthetized cats in response to both a speech utterance and sinusoidally-modulated broadband noise. Modulation transfer functions (MTF) were derived from the magnitude and phase of the responses to noise. MTFs were then inverse Fourier transformed and temporally integrated to obtain the MTF step response. MTF step responses of most AN fibers were monophasic and resembled tone-burst response patterns. While most CN cells had monophasic step responses like those of AN fibers, a minority had biphasic step responses, with a short (< 50 msec) positive phase followed by a long negative phase possibly reflecting inhibition. In the IC,

biphasic step responses were much more common than in the CN and often showed pronounced negative phases. For IC cells, the MTF step response was correlated with responses to the speech utterance: Units with monophasic step responses tended to show a tonic response throughout each syllable, while units with biphasic step responses tended to show a phasic response primarily restricted to syllable onsets.

These results show that, while units at all three locations encode the perceptually-important envelope modulations of speech in their discharge patterns, a major transformation occurs between the CN and the IC. The MTF step response may provide a unit classification scheme that reveals phenomena occuring on slow time scales, making it well suited for predicting neural responses to the temporal envelope of speech.

1.4.3 Circuit Model of Onset Cells in the Cochlear Nucleus

Rapid acoustic transients are known to be important in speech perception. Thus, neurons in the cochlear nucleus (CN) that respond to these transients (onset responders) may have an important role in speech coding.

We have developed a single-node circuit model of CN onset cells which is constrained by measured responses to tones and noise. Inputs to the model neuron are exclusively excitatory and derive from model auditory-nerve (AN) fibers. The model must have the following properties to capture both the phasic response of onset cells to high-frequency tone and noise bursts and the precise phase-locking to low-frequency tones: (1) fast membrane integration and spike recovery dynamics (< 1 ms), (2) many independent AN inputs (> 50) that are individually ineffective in driving the model cell, and (3) AN inputs from a wide range of characteristic frequencies (CF). These model characteristics are consistent with connectivity patterns derived from anatomical studies and electrical properties derived from brain slices.

Simulation of a population of onset cells in response to natural speech predicts that high-CF onset cells discharge in response to rapid transients, such as the release of plosives, while low-CF cells discharge on every cycle of the fundamental frequency of vowels. These results suggest that the CN onset population enhances perceptually-important speech features.

1.4.4 Publications

Journal Articles

Cariani, P.A., and B. Delgutte. "Neural Correlates of the Pitch of Complex Tones. I. Pitch and Pitch Salience." *J. Neurophysiol.* 76: 1698-1716, 1996.

Cariani, P.A., and B. Delgutte. "Neural Correlates of the Pitch of Complex Tones. II. Pitch Shift, Pitch Ambiguity, Phase Invariance, Pitch Circularity, Rate Pitch and the Dominance Region for Pitch." *J. Neurophysiol.* 76: 1717-1734, 1996.

Delgutte, B. "Physiological Models for Basic Auditory Percepts." In *Auditory Computations.* Eds. H. Hawkins and T. McMullen. New York: Springer-Verlag, 1996; pp. 157-220.

Kelly, O.E., D.H. Johnson, B. Delgutte, and P.A. Cariani. "Fractal Noise Strength in Auditory-nerve Fiber Recordings." *J. Acoust. Soc. Am.* 99: 2210-2220 (1996).

Conference Papers

Delgutte, B., B.M. Hammond, S. Kalluri, L.M. Litvak, and P.A. Cariani. "Neural Encoding of Temporal Envelope and Temporal Interactions in Speech." Workshop on Auditory Basis of Speech Perception, Keele, United Kingdom, July 1996.

Delgutte, B., B.M. Hammond, and P.A. Cariani. "Neural Coding of the Temporal Envelope of Speech: Relation to Modulation Transfer Functions." *Abstr. Assoc. Res. Otolaryngol.* 20, 1997. Forthcoming.

Hammond, B.M., W.M. Rabinowitz, and B. Delgutte. "Modulation Transfer Functions of Auditory-nerve Fibers: Measurements and Use in Predicting the Neural Response to Speech." *Abstr. Assoc. Res. Otolaryngol.* 19: 78, 1996.

Hammond, B.M., W.M. Rabinowitz, and B. Delgutte. "Use of Modulation Transfer Functions to Predict the Response of Auditory-nerve Fibers to Speech." *Workshop on Auditory Basis of Speech Perception*, Keele, United Kingdom, July 1996.

Hirahara, T., P.A. Cariani, and B. Delgutte. "Representation of Low-frequency Vowel Formants in the Auditory Nerve." *Abstr. Assoc. Res. Otolaryngol.* 19: 80 (1996).

Hirahara, T., P.A. Cariani, and B. Delgutte. "Representation of Low-frequency Vowel Formants in

the Auditory Nerve." *Proceedings of the Workshop on Auditory Basis of Speech Perception*, Keele, United Kingdom, July 1996, pp. 83-86.

Kalluri, S., and B. Delgutte, "A General Model of Spiking Neurons Applied to onset Responders in the Cochlear Nucleus." *Computational Neuroscience Meeting*, Cambridge, Massachusetts, July 1996.

Kalluri, S., and B. Delgutte, "An Electrical Circuit Model for Cochlear Nucleus onset Responders." *Abstr. Assoc. Res. Otolaryngol.* 20, 1997.

Tsai, E.J., and B. Delgutte, "Neural Mechanisms Underlying Intensity Discrimination: Responses of Auditory-nerve Fibers to Pure Tones in Band-reject Noise." *Abstr. Assoc. Res. Otolaryngol.* 20, 1997.

1.5 Cochlear Efferent System

Sponsor

National Institutes of Health
Grant RO1 DC00235

Project Staff

Dr. John J. Guinan, Jr., Dr. Christopher A. Shera, Konstantina M. Stankovic

Our goals are to understand the mechanisms by which medial efferents act and the resulting modifications of sound coding in auditory-nerve fibers. The aims include: (1) testing the efferent-shunt hypothesis by determining whether its predictions hold, (2) recording from single medial-efferent fibers to determine the percentage that fire in response to shocks, (3) testing the extent to which efferent inhibition at low sound levels is due to a depression of the gain of the cochlear amplifier, (4) measuring medial-efferent inhibition of single-auditory-nerve-fiber responses to high-level sounds to determine its dependence on shock stimulation parameters and sound frequency relative to the characteristic frequency (CF), and (5) testing the hypothesis that medial-efferent inhibition at high sound levels is mediated electrically by mimicing the efferent-induced change in endocochlear potential (EP) with current injected into scala media and determining whether this mimics efferent inhibition at high sound levels.

1.5.1 Studies and Results

Work begun during the previous funding period and finished during the past year describe new results on efferent effects at high sound levels.[9] Previous work had shown that medial efferents can inhibit responses of auditory-nerve fibers to high-level sounds and that fibers with low spontaneous rates (SRs) are inhibited most. However, quantitative interpretation of those data was made difficult by effects of adaptation. To minimize systematic differences in adaptation, we measured efferent inhibition with a randomized presentation of both sound level and efferent stimulation. In anesthetized cats, we stimulated efferents with 200/s shocks and recorded auditory-nerve-fiber responses to tone bursts (0-100 dB SPL, 5 dB steps) at their CFs. Below 50 dB SPL, efferent inhibition (measured as equivalent attenuation) was similar for all fibers with similar CFs in the same cat. At 45-75 dB SPL, low-SR and medium-SR fibers often showed much larger inhibition, and substantial inhibition even at 100 dB SPL. Expressed as a fractional decrease in rate, at 90-100 dB SPL the inhibition was 0 percent, 6 percent and 13 percent for high-, medium-, and low-SR fibers. Finding the largest equivalent attenuations at 45-75 dB SPL does not fit with the hypothesis that medial-efferent inhibition is due solely to a reduction of basilar-membrane motion. The large attenuations, some over 50 dB, indicate that medial efferent inhibition is more potent than previously reported.

We have published a preliminary test of the efferent-shunt hypothesis.[10] It is widely believed that outer-hair-cell (OHC) fast motility acts to amplify basilar membrane motion. Since OHC fast motility is controlled by the voltage across the OHC membrane, efferent synapses may inhibit by shunting OHC receptor currents thereby reducing OHC motion. For such a shunt to produce substantial inhibition, the OHC synaptic conductance must exceed the OHC non-synaptic admittance which increases approximately in proportion to frequency, for frequencies above about 1 kHz. This prediction was tested in anesthetized cats by measuring the

---

[9] Guinan, J.J., Jr., and K.M. Stankovic. "Medial Efferent Inhibition Produces the Largest Equivalent Attenuations at Moderate to High Sound Levels in Cat Auditory-nerve Fibers." *J. Acoust. Soc. Am.* 100: 1680-1690 (1996).

[10] Guinan, J.J., Jr. "Efferent Inhibition as a Function of Efferent Stimulation Parameters and Sound Frequency: Testing the OHC-shunt Hypothesis." In *Diversity in Auditory Mechanics*. Ed: E.R. Lewis, G.R. Long, R.F. Lyon, P.M. Narins, C.R. Steele, Singapore: World Scientific. Forthcoming.

inhibition produced by stimulation of medial efferents on tone-pip-evoked compound action potentials (CAPs). In preliminary results, for a given shock rate, the shock level which produced a 10 percent CAP reduction increased dramatically with sound frequency for two cats, but on a third cat, it increased only for low-shock rates. Thus most of the data are consistent with the OHC-shunt hypothesis. In addition, our data provide a fundamentally new view of the parametric dependence of efferent inhibition that is not consistent the current view (obtained from experiments using clicks) that the growth of efferent inhibition with increased efferent firing is independent of sound frequency. The parametric dependence of efferent inhibition has been the focus of our recent work in this area.[11]

Our work to test the extent to which efferent inhibition at low sound levels is due to a depression of the gain of the cochlear amplifier (Aim 1c) has concentrated on developing and testing the methods to measure the gain of the cochlear amplifier. In a recent abstract,[12] we present a method, inspired by the work of Allen and Fahey[13] by which cochlear amplification and nonlinearity can be explored noninvasively using distortion-product otoacoustic emissions as an intracochlear "sound source." Our preliminary results differ in important respects from the data reported by Allen and Fahey.[13] In particular, we find evidence of significant amplification in a broad region basal to the peak of the traveling wave. We are still explorinng the possible reasons for the different results, including the influences of confounding effects such as two-tone suppression.

We have explored efferent effects on auditory-nerve responses to tail-frequency tones in an effort to determine whether there is efferent inhibition without a depression of basilar-membrane motion.[14] Stimulation of medial olivocochlear (MOC) efferents that synapse on outer hair cells reduces auditory-nerve activity in fibers that contact inner hair cells. Possible mechanisms for this effect can be grouped into two broad categories: (1) efferent inhibition of basilar-membrane (BM) motion, and (2) efferent modulation through pathways that do not change BM motion (e.g., efferent effects on endocochlear potential or other cochlear potentials, or changes in cochlear micromechanics). We have focused on experimental conditions under which there is no reported change in BM motion.[15] Specifically, we measured efferent effects on single auditory-nerve fibers (ANF) stimulated in the broadly-tuned low-frequency "tail" region of tuning curves. We measured randomized rate-level functions from cat ANFs with high CFs (CF $\geq$ 5 kHz), stimulated with tones at least two octaves below CF. Our results indicate that electrical stimulation of MOC efferents can indeed inhibit ANF responses to tail-frequency tones. The magnitude of efferent inhibition (expressed as efferent-induced level shift) was quite variable, ranging from 0-14 dB. Efferent inhibition depended on both sound level (often being largest close to threshold) and frequency. On the average, inhibition of high-CF ANFs responding to 1 kHz tones was around 5 dB. ANFs with hypersensitive tails (seen in ears with compromised function) were especially susceptible to efferent inhibition at tail frequencies. In guinea pigs, efferent stimulation "had no apparent effect on BM displacement in response to tones at frequencies more than one-half an octave below CF."[15] If such results hold for cats, our results suggest that at tail frequencies, efferents may exert their effect on ANFs through one or more of the alternative, as yet unidentified, mechanisms.

During the current period, we revised a manuscript which describes, for a clinical audience, our previously reported finding of a class of primary vestibular afferents in the cat which are responsive to sounds at moderately intense sound levels.[16]

---

[11] Guinan, J.J., Jr. "Efferent Inhibition as a Function of Efferent Shock Rate, Shock Level and Sound Frequency: Testing the OHC-shunt Hypothesis." *Association for Research in Otolaryngology, Abstracts* 20: 10 (1997).

[12] Shera, C.A., and J.J. Guinan, Jr. "Measuring Cochlear Amplification and Nonlinearity using Distortion-Product Otoacoustic Emissions as a Calibrated Intracochlear Sound Source." *Association for Research in Otolaryngology, Abstracts* 20: 13 (1997).

[13] Allen and Fahey, *J. Acoust. Soc. Am.* 92:178-188 (1992).

[14] Stankovic, K.M, and J.J. Guinan, Jr. "Efferent Effects on Auditory-nerve Responses to Tail-frequency Tones: Inhibition without Altering Basilar-membrane Motion?" *Association for Research in Otolaryngology, Abstracts* 20: 155 (1997).

[15] Murugasu and Russell, *J. Neurosci.* 16: 325-332 (1996).

[16] McCue, M.P., and J.J. Guinan Jr. "Sound-Evoked Activity in Primary Afferent Neurons of a Mammalian Vestibular System." *Am. J. Otol.* 18: 355-360 (1997).

1.5.2 Publications

Guinan, J.J., Jr. "Efferent Inhibition as a Function of Efferent Shock Rate, Shock Level and Sound Frequency: Testing the OHC-shunt Hypothesis." *Association for Research in Otolaryngology, Abstracts* 20: 10 (1997).

Guinan, J.J., Jr. "Efferent Inhibition as a Function of Efferent Stimulation Parameters and Sound Frequency: Testing the OHC-shunt Hypothesis." In *Diversity in Auditory Mechanics.* Eds. E.R. Lewis, G.R. Long, R.F. Lyon, P.M. Narins, and C.R. Steele, Singapore: World Scientific. Forthcoming.

Guinan, J.J., Jr., and K.M. Stankovic. "Medial Efferent Inhibition Poduces the Largest Equivalent Attenuations at Moderate to High Sound Levels in Cat Auditory-nerve Fibers." *J. Acoust. Soc. Am.* 100: 1680-1690 (1996).

McCue, M.P., and J.J. Guinan Jr. "Sound-Evoked Activity in Primary Afferent Neurons of a Mammalian Vestibular System." *Am. J. Otol.* 18: 355-360 (1997).

Shera, C.A., and J.J. Guinan, Jr. "Measuring Cochlear Amplification and Nonlinearity using Distortion-Product Otoacoustic Emissions as a Calibrated Intracochlear Sound Source." *Association for Research in Otolaryngology, Abstracts* 20: 13 (1997).

Stankovic, K.M, and J.J. Guinan, Jr. "Efferent Effects on Auditory-nerve Responses to Tail-frequency Tones: Inhibition without Altering Basilar-membrane Motion?" *Association for Research in Otolaryngology, Abstracts* 20: 155 (1997).

1.6 Cochlear Implants

Sponsor

National Institutes of Health
Grant P01-DC00361
Contract N01-DC-6-2100

Project Staff

Dr. Donald K. Eddington, Dr. Colette Boex-Spano, Dr. William M. Rabinowitz, Joseph Tierney

1.6.1 Introduction

The basic function of a cochlear prosthesis is to provide a measure of hearing to the deaf by using stimulating electrodes implanted in or around the cochlea to elicit patterns of spike activity on the array of surviving auditory-nerve fibers. By modulating the patterns of neural activity, these devices attempt to present information that the implanted patient can learn to interpret. The overall goal of our work is two-fold: (1) to understand the mechanisms responsible for the neural activity patterns elicited by electric stimulation, and (2) to use this understanding to design wearable sound processors that translate acoustic signals into electric stimuli that produce sound sensations deaf subjects can interpret. This year, our report concentrates on one area of sound processor design: the mapping of acoustic level to electric stimulation level.

1.6.2 Standard Cochlear Implant Mapping Functions

Because the dynamic range of sound intensity is at least four orders of magnitude larger than the dynamic range of electric stimulus level for most cochlear implant users, the method used to map acoustic level to electric stimulus level is a key component of any sound processor. Figure 7 shows a block diagram that emphasizes the level-mapping components of a sound processing system commonly used to stimulate intracochlear electrodes.[17] We implemented the microphone output so that it is processed by N (typically six or eight) parallel channels, each associated with a particular electrode implanted in the cochlea.[18] Using

[17] B.S. Wilson, C.C. Finley, D.T. Lawson, R.D. Wolford, D.K. Eddington, and W.M. Rabinowitz, "Better Speech Recongition with Cochlear Implants," *Nature* 352: 236-238 (1991).

[18] D.K. Eddington, J. Tierney, W.M. Rabinowitz, V.A. Noel, M.E. Whearty, L. Delhorne, and N. Garcia, Speech Processors for Auditory Prostheses, First Quarterly Progress Report to NIH, (Cambridge: MIT Research Laboratory of Electronics, 1996); D.K. Eddington, L.

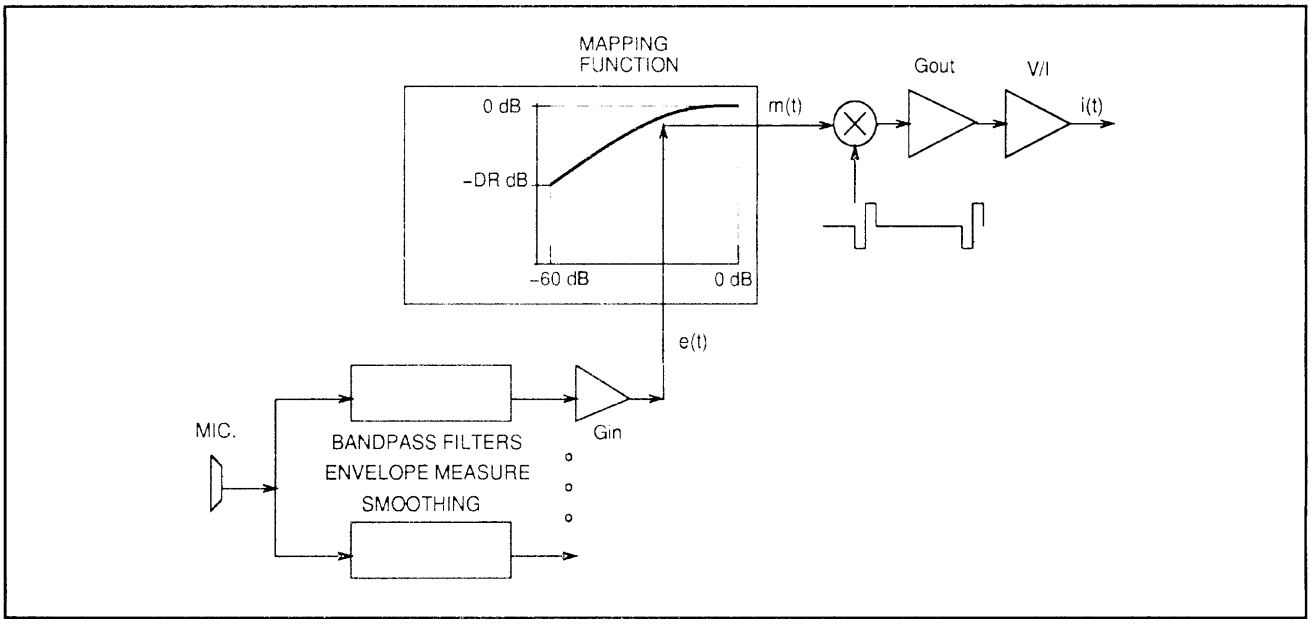

Figure 7. Block diagram of a cochlear implant sound processing system that emphasizes the level mapping stage. For each channel's center frequency, the total gain before the mapper is characterized by a single input gain (Gin). DR represents the output dynamic range. The mapper output amplitude modulates a pulse train that is converted to a current stimulus by the voltage-to-current source converter (V/I).

bandpass filters, the channels split the sound spectrum into N contiguous and logarithmically spaced segments with the channel-to-electrode assignment determined by the longitudinal position of each electrode in the cochlea (e.g., assignment of the lowest frequency channel to the most apical electrode and the highest frequency channel to the most basal electrode). After the bandpass filter, each channel employs a stage of rectification and lowpass filtering or quadrature detection to extract the band envelope. This envelope is presented to the level mapper, and the "compressed" result is used to modulate the amplitude of a pulse train that becomes the current waveform used to stimulate the channel's implanted electrode.

The input gain (Gin) determines the range of envelope levels that will fall within the 60 dB input range that is mapped in each channel. Gin is constant across channels and is set so that 1 percent of the envelope levels will be clipped in the channel with the most energy when the TIMIT[19] database of speech materials is played at a conversational level.

The output dynamic range (DR in figure 7) is determined for each channel based on the psychophysical threshold (THR) and most comfortable (MCL) stimulus levels measured using the electrode associated with that channel. The stimulus waveform used to make these measurements roughly corresponds to that used by the processor of interest (e.g., biphasic, cathodic-first pulse train, 2000 Hz repetition rate, 31.25 μs/phase, 50 ms overall duration).

The standard function used by commercial sound processors to map the input range to the output range is logarithmic. As a result, with an input mapping range of 60 dB, each 10 dB change in envelope level changes the output current level by one-sixth of the range from THR to MCL.

Figure 8 shows magnitude estimates for loudness made by an implantee using the standard logarithmic mapping function together with a line representing magnitude estimates of normal hearing listeners for a 1 kHz tone. (The methods used to obtain the magnitude estimates are given in the figure caption.) Results like these indicate that loudness grows very differently for implant subjects using standard mapping functions than it does for normal hearing listeners. In order to determine whether sound processing systems that more

Delhorne, N. Garcia, V.A. Noel, W.M. Rabinowitz, J. Tierney, and M.E. Whearty, Speech Processors for Auditory Prostheses, Second Quarterly Progress Report to NIH, (Cambridge: MIT Research Laboratory of Electronics, 1996).

[19] W.M. Fisher, G.R. Doddington, and K.M. Goodie-Marshall "The DARPA Speech Recognition Research Database: Specifications and Status," DARPA Workshop on Speech Recognition, Palo Alto, California, 1986.

closely approximate normal loudness growth will improve speech reception for implantees, we are developing methods to guide the design of mapping functions for CIS processors that restore the normal growth of loudness.

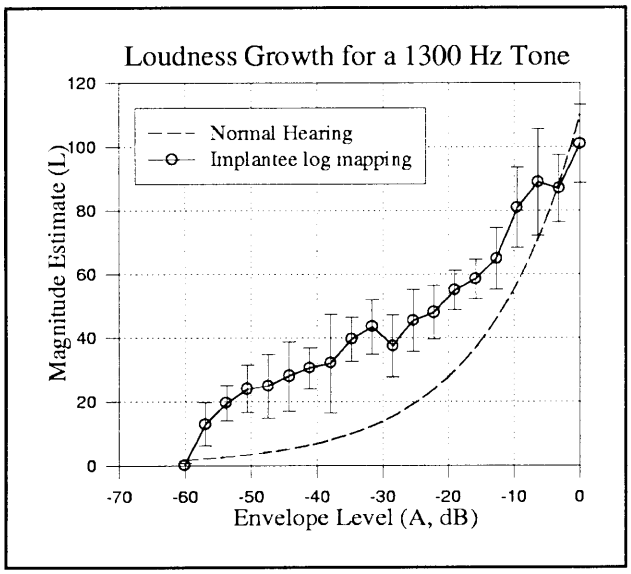

Figure 8. Comparison of loudness growth (magnitude estimates) for implant subject S01 using our standard laboratory sound processor with loudness growth for normal hearing subjects. Error bars correspond to ± one standard deviation. In the case of the implantee, magnitude estimates were obtained for 20 levels of a 1300 Hz tone (center frequency for channel 3) presented to the external input of the processor. The twenty levels were logarithmically distributed over the 60 dB range shown in the figure. Each level was presented ten times in pseudo random order. A presentation consists of two 300 ms tones separated by approximately 300 ms.

The dashed line depicting normal loudness growth was plotted using the relationship $L = kP^{0.6}$, where L represents loudness and P represents acoustic pressure. The acoustic level used as the reference (0 dB) produced loudness magnitude estimates in normal hearing subjects that correspond to those of the implant subject for electric stimulation levels at MCL.

1.6.3 Mapping Functions that Restore Normal Loudness Growth

Our method for designing "normal loudness growth" (NLG) mapping functions uses the relationship between loudness and the sound pressure of single tones measured in normal hearing subjects and the relationship between loudness and electric stimulus level measured at individual electrodes in implantees to derive a set of mapping functions that restore normal loudness growth for single tones at the center frequencies of the processor channels.

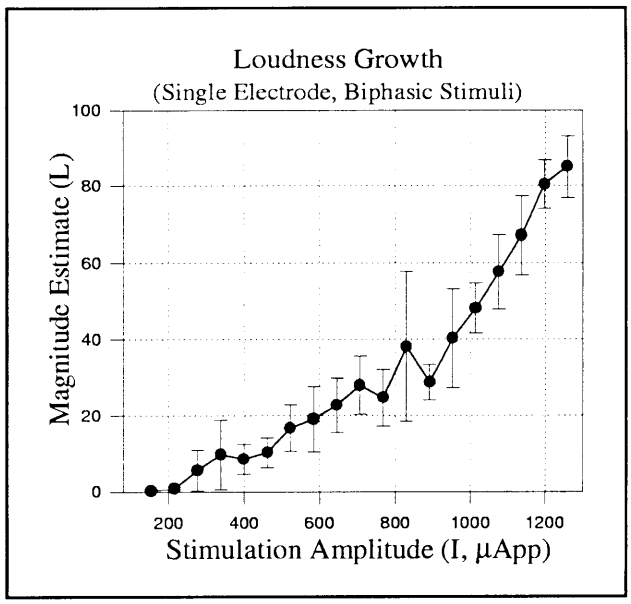

Figure 9. Magnitude estimates obtained from subject S01 when stimulating electrode 3 using 20 levels ranging from THR to MCL. The biphasic, stimulus waveform (cathodic-first, 31.25 μs/phase, 2000 Hz, 300 ms) was produced directly by controlling a programmable current source. The error bars represent ± one standard deviation.

The first step of this process is to obtain loudness growth functions for each of the implantee's electrodes. Figure 9 shows an example of measurements made to determine this function for subject S01's electrode 3. The magnitude estimation task is like that described in the caption of figure 8 and the stimulus waveform was the same described above for the measurement of THR and MCL except that the duration is 300 ms instead of 50 ms. Once the magnitude estimates are obtained for each electrode, they can be fit to give a loudness growth function, $L_e(I)$, of the form

$$L_e = a_{0,e} + a_{1,e}I + a_{2,e}I^2 + a_{3,e}I^3 + a_{4,e}I^4 \quad (1)$$

where L_e is the loudness produced by stimulating electrode "e" at stimulus level I. A maximum current is selected for each electrode ($I_{e,max}$) corresponding to a loudness magnitude (L_{max}) that is constant across electrodes. Next, using the normal loudness growth function $L = kP^{0.6}$, the relation between the logarithm of the ratios of loudness and sound pressure (P) can be expressed as

$$\log(L_i/L_{max}) = 0.6 * \log(P_i/P_{max}) \quad (2)$$

Because the sound pressure (P) of a tone at the center frequency of channel "c" is linearly related to

the envelope amplitude in the channel (E_c) equation 2 can be rewritten as

$$L_{c,i} = L_{max}*(E_{c,i}/E_{max})^{0.6} \quad (3)$$

Using equation 3 and equation 1, a mapping function can be computed that specifies the relationship between current level and envelope amplitude, $I_e(E_c)$, that produces normal loudness growth for a tone presented at the center frequency of a particular channel. The resulting mapping function for S01's channel 3 (connected to electrode 3) is shown together with the standard logarithmic mapping function in the top panel of figure 10. It is clear that the two mapping functions differ greatly.

In order to test the method described above, we measured magnitude estimates for tone stimuli in subjects using CIS processors with NLG mapping functions and compared them to normal loudness growth functions. The bottom panel of figure 10 shows a representative example of such results. Magnitude estimates obtained from subject S01 using a 1300 Hz tone burst (center frequency for channel 3) are plotted for both the standard mapping function (open symbols) and the mapping function designed to restore normal loudness growth (closed symbols). Notice that the overall growth of loudness exhibited by the magnitude estimates made using the NLG mapping function is very similar to the growth of loudness for normal listeners represented by the dashed line.

Table 1: 16-Consonant Indentification.

Subject	Standard Logarithmic Mapping (Percent Correct)	Normal Loudness Growth Mapping (Percent Correct)
S01	77	80
S22	65	81

While the NLG mapping functions derived using this method are based on single tones at a channel's center frequency, we are interested in their effect on speech reception. Table 1 shows preliminary results from evaluating the ability of two subjects to identify 16 consonants.[20] The mean scores represent at least 15 randomized presentations of the 16 consonant lists for both the standard logarithm and NLG mapping functions. Subject S01's scores are similar with both mappings for these acute, laboratory tests. Although subject S22 shows a marked improvement for the NLG mapping, this result must be considered preliminary since the THR and MCL parameters used to define the standard mapping function were measured several months earlier.

We plan to test whether NLG mapping functions improve speech reception by substituting wearable processors that use NLG mapping functions for the standard sound processor worn by seven subjects. Once these subjects have reached asymptotic performance on a battery of standard speech reception tests, we will compare their performance using the standard and NLG mapping functions. We also plan to conduct additional laboratory studies using NLG mapping functions to determine how loudness grows for tone frequencies positioned at the boundary of two processor channels and for broader band inputs like speech and speech-shaped noise. We hope that these investigations will lead to refined NLG mapping functions that will improve the listening experience for cochlear implant users.

[20] R.S. Tyler, J.P. Preece, and N. Tye-Murray, "Iowa Audiovisual Speech Perception Laser Videodisc," (Iowa City: University of Iowa, 1987).

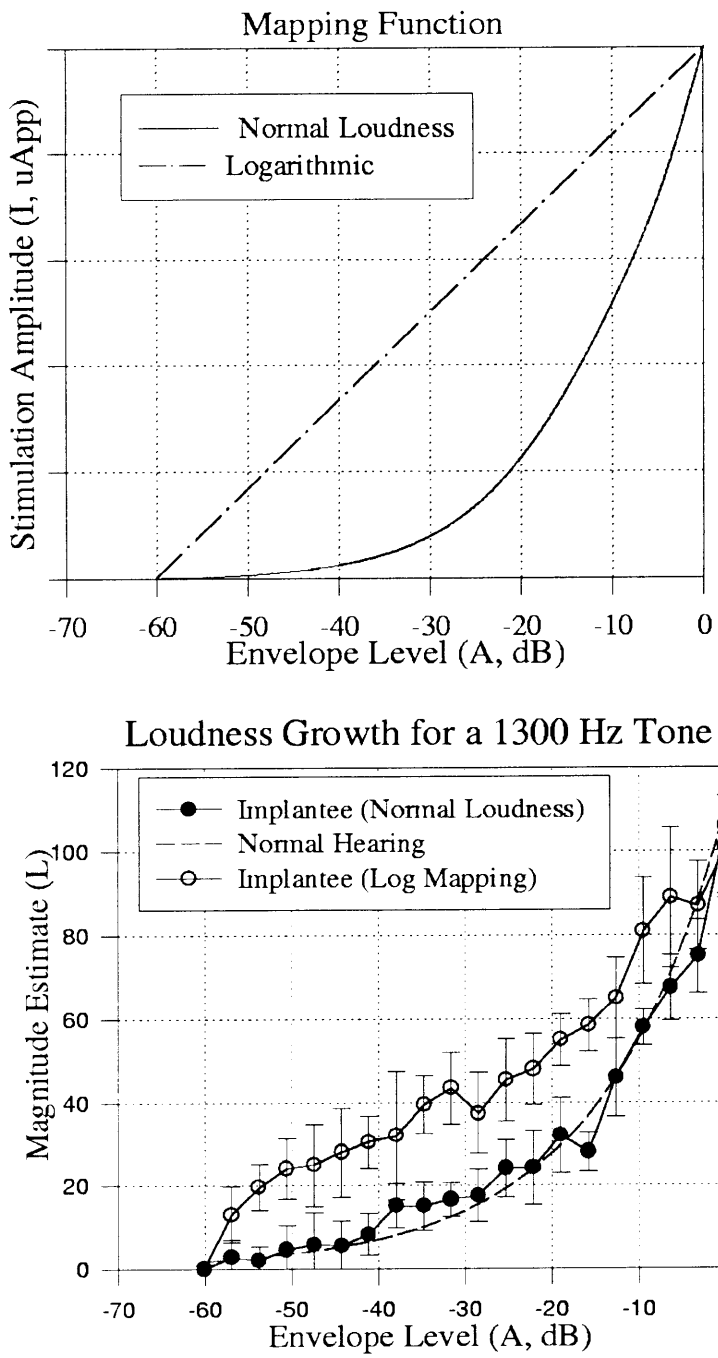

Figure 10. The top panel shows two mapping functions for S01's channel 3. The solid line represents the function designed to restore normal loudness growth and the broken line represents the standard logarithmic mapping function. The bottom panel plots magnitude estimates obtained from subject S01 using a 1300 Hz tone burst (center frequency for channel 3) for both the standard mapping function (open symbols) and the mapping function designed to restore normal loudness growth (closed symbols). The dashed line represents loudness growth for normal hearing listeners for 1 kHz acoustic tones.